

# HIGH-POWER BEAM TEST OF THE APS GRAZING-INCIDENCE INSERTION DEVICE X-RAY BEAM POSITION MONITOR\*

B.X. Yang, G. Decker, S. H. Lee, P. Den Hartog, T.-L. Kruey, J. Collins, M. Ramanathan, and N. G. Kujala, APS, ANL, Argonne, IL 60439, USA

## Abstract

We present test results of a grazing-incidence insertion device x-ray beam position monitor (GRID-XBPM) at beamline 29-ID. In the vertical direction, the XBPM readout showed little gap dependence for the total undulator beam power from 17 W to 10.6 kW, covering nearly three decades, as one expects from center-of-mass measurements. In the horizontal direction, the calibration factor shows strong gap dependence, as predicted by computer simulations. The XBPM will work reliably near its center position. Monochromatic beam profiles were measured using a liquid-nitrogen-cooled Si (111) double-crystal monochromator. Their centers correlate strongly with the white-beam positions derived by the XBPM using x-ray fluorescence (XRF). We demonstrated experimentally that the x-ray beam from two different undulators can be centered on the XBPM aperture reliably and reproducibly. Thermal measurements found a maximum of ~ 15°C temperature rise in the chamber walls with the time constant ~ 10 minutes.

## INTRODUCTION

A grazing-incidence insertion device x-ray beam position monitor (GRID-XBPM) has been under design and construction at the APS for the past two years [1,2]. At 0.8 degree grazing-incidence angle, the XBPM assembly was designed to withstand two inline Undulators A at 150-mA beam current, with a total power of 16 kW. This XBPM was recently tested for the first time with two undulators, each 2.4 m long with a 3.3 cm period, at beamline 29ID, at up to 50% of its design capacity.

## TEST SETUP

Figure 1 show the test setup: At fully closed gap, the white undulator x-ray beam (shown in red) is ~ 10 mm (H) × 5 mm (V) at the exit of the front end (FE), 25 m from the source, compared with the FE exit aperture of 5 mm × 6 mm. The XBPM consists of two vertical, water-cooled GlidCop plates intercepting the beam in grazing incidence. The exit aperture of the XBPM assembly is adjustable and was set to 2, 3, and 4 mm during the tests to assess the differences. Two detector assemblies (AB and CD) are mounted opposite to the plates to measure the XRF intensity and the vertical coordinates of the XRF footprint [1]. Since the XRF intensity is too strong for the silicon PIN diode to be exposed to it directly, stainless steel plates were used to down-convert the XRF intensity by ~100-fold so silicon

PIN diodes can be used in photo-voltaic mode to read out the signals.

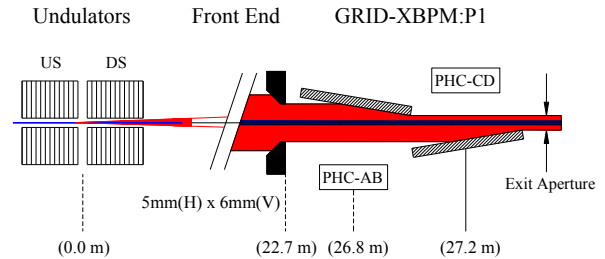


Figure 1: GRID-XBPM beam test in 29-IDA (top view).

## XBPM TEST DATA

### Signal-to-Background Measurements

First, we scan the electron beam horizontally to record the bend magnet background with the undulator gap wide open ( $G_{max}=180$  mm) and then measure the undulator signal at a gap  $G$  of 29 mm ( $K\sim 0.4$ ). The upper panel of Fig. 2 shows the measured XRF intensities as functions of the horizontal e-beam angle from the inboard (AB) and outboard (CD) detectors. For clarity, the background signal was enlarged by 100-fold. For comparison, the lower panel shows the photoemission (PE) current from our existing Au-coated XBPM in Sector 7. We can make the following observations from these figures:

- The photoemission current clearly shows higher background level, especially beyond the half angle of Decker Distortion,  $\pm 0.5$  mrad [3]. The signal-to-background ratio is ~ 3:2 during operations.
- The Cu XRF signal has a narrower peak and generates ~50% less current than the PE blades at the peak, but its background is lower by a factor of 100.

While a constant background can be subtracted in data processing, variations of the background add uncertainty to position measurements. At the same time, a strong dependence of undulator signal on position increases sensitivity of the measurements. Hence, the ratio of background-to-undulator signal slopes can be used to measure the impact of the background,

$$\epsilon_x = \frac{|AB'(G_{max})| + |CD'(G_{max})|}{|AB'(G)| + |CD'(G)|} \quad (1)$$

\*Work supported by Argonne, a U.S. Department of Energy Office of Science, under Contract No. DE-AC02-CH11357.

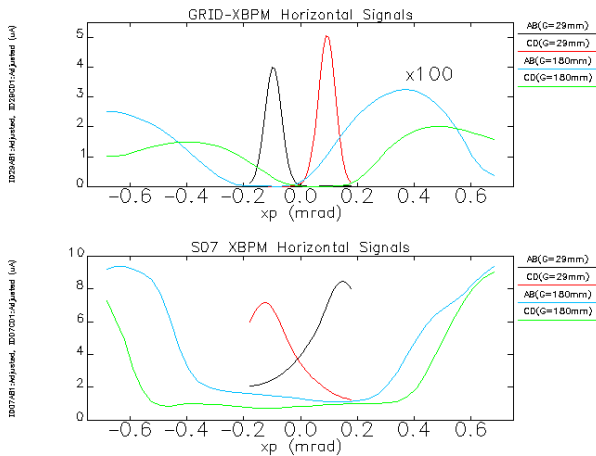


Figure 2: Wide-angle scan data gap = 29 mm: top is from GRID-XBPM with background enhanced by 100-fold; bottom is from Au-coated blades.

The smaller this ratio, the lower is the background's impact. Figure 3 shows the measured slope ratio of several Au-coated XBPMs of different design, along with those of the GRID-XBPM with different exit apertures. The GRID-XBPM is clearly superior by one to two orders of magnitude. A smaller exit aperture is especially advantageous for large-gap (low-*K*) undulator operations.

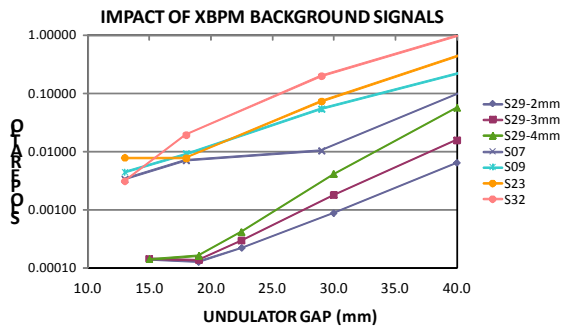


Figure 3: Background-to-undulator signal slope (BUSS) ratio for selected Au-PE XBPM and GRID-XBPM with 2-, 3-, and 4-mm exit aperture.

**Vertical Center-of-Mass Measurements**

By design, vertical positions of the x-ray beam are obtained from the center-of-mass of the XRF footprint on the XBPM plates [1]. Figure 4 shows the measured vertical positions as functions of undulator gap for nine different vertical e-beam angle settings. Since the diode current ranges from 10 nA to 50  $\mu$ A, the gains of the current amplifiers were changed three times during the scan, which resulted in as many steps in the data, indicating that an amplifier with wider dynamic range is desirable. From the data taken at 10  $\mu$ rad above and below the axis, we derived the calibration factor *k* and offset *y*<sub>0</sub> of the XBPM, as plotted in Figure 5. We found an overall  $\pm 2\%$  change in *k*, which is likely due to imperfections of component fabrication and alignment. We can also see a systematic difference in vertical offsets

between the upstream and downstream undulators. This is likely due to differences in their steering from magnetic field errors.

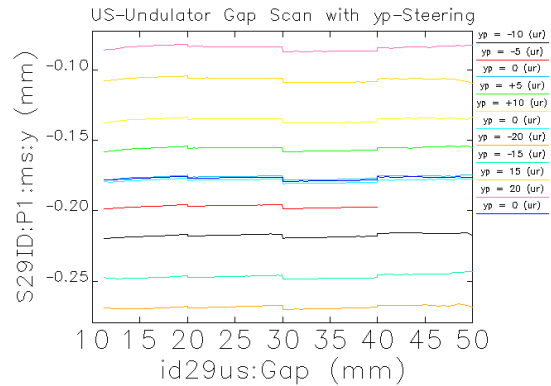


Figure 4: Undulator gap scan for selected beam angles.

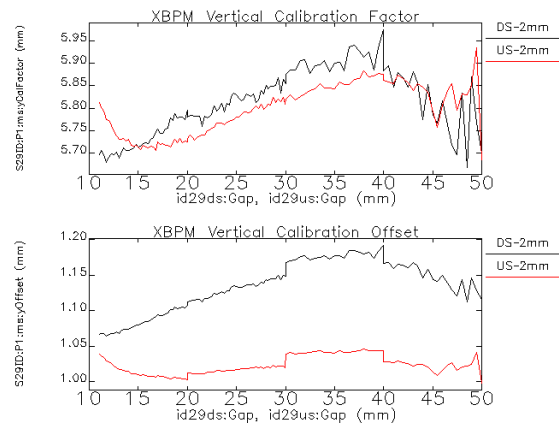


Figure 5: Vertical calibration constants derived from gap scan: Upper panel shows the calibration factor *k*, and lower panel shows the offset *y*<sub>0</sub>.

**Horizontal Calibration**

By design, the horizontal position of the beam is obtained from the ratio of the difference in x-ray intensities intercepted by the inboard and outboard absorbers over their sums,  $x = k(\Delta/\Sigma) + x_0$ . Similar to Figure 4, we derived the horizontal calibration factor *k* and offset *x*<sub>0</sub> from the data taken at 5  $\mu$ rad inboard and outboard from the axis and show them in Figure 6. Since these scans are taken over several hours, some drift of the orbit may have happened and the calibration factors for upstream and downstream undulators are not identical. But the trend is clear: As the gap is closed, the horizontal beam size increases, and the calibration factor increases proportionally [2]. Eventually, the beam overfills the front-end aperture and XBPM is no longer sensitive to the beam position ( $k = \infty$ ). From the horizontal offset data, we can see that the two undulator beams do not coincide, but the two beam spots are closer in the horizontal direction than in the vertical direction. We also note that due to the high position sensitivity ( $k < 1$  mm), the noise in the position (offset) data is low in calibrated units, easily in the micrometer range.

Copyright © 2012 CC-BY-3.0 and by the respective authors

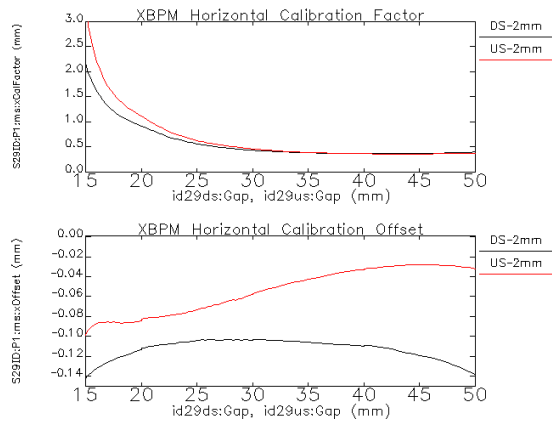


Figure 6: Horizontal calibration constants derived from gap scan data: Upper panel shows the calibration factor  $k$ , and lower panel shows the offset  $x_0$ .

### Monochromatic Beam Measurements

Figures 5 and 6 revealed evidence that x-rays from the two undulators may be striking the XBPM at different locations while the e-beam is pinned down at identical positions at the RFBPMs. To confirm this observation, we used the setup shown in Figure 7 to measure the vertical beam profiles: the undulator gap was set to 25 mm; the slits openings were set to 1 mm (H)  $\times$  0.3 mm (V); the first Si(111) crystal, cooled by LN<sub>2</sub>, was set to reflect the first harmonic photon beam and the second crystal was tweaked to maximize the downstream ion chamber current. We closed the gap an undulator at a time and scanned the electron beam angle upwards and downwards across the slits to assess instrument asymmetry/drift. Figure 7 shows the measured profiles. A separation of profiles by 90  $\mu$ m was obtained by curve fitting, in good agreement with Fig. 5. Additional tests with position feedback using XBPM showed that the monochromatic beam can be positioned accurately and reproducibly through a narrow aperture when the two undulators are switched.

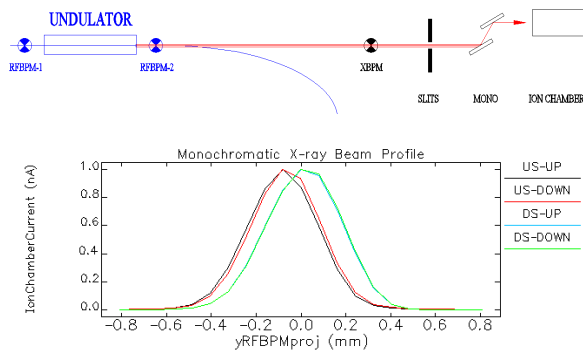


Figure 7: Upper panel: Setup for monochromatic beam profile measurement. Lower panels: First harmonic monochromatic beam profiles from upstream (US) and downstream (DS) undulators measured with e-beam scanning upwards (UP) and downwards (DOWN).

### Thermal Transient Measurements

During normal operations, the GRID-XBPM intercepts up to 10 kW, a major portion of the undulator power in high-heatload front ends. It is thus natural to be concerned about its thermal stability. Figure 8 shows an initial assessment of the thermal effect: the XBPM readout and the power carried by the cooling water were recorded at 1-s intervals before and after the photon shutter is opened. It takes about 5 minutes for the power to reach a steady state, indicating the time required to heat up the GlidCop body. Additional thermal imaging found  $\sim 15^\circ\text{C}$  temperature rise in the chamber walls with the time constant  $\sim 10$  minutes. As the components heat up, their upwards movement and deformation causes the XBPM readout to shift downwards by as much as 12  $\mu$ m, until a steady state is reached in  $\sim 15$  minutes.

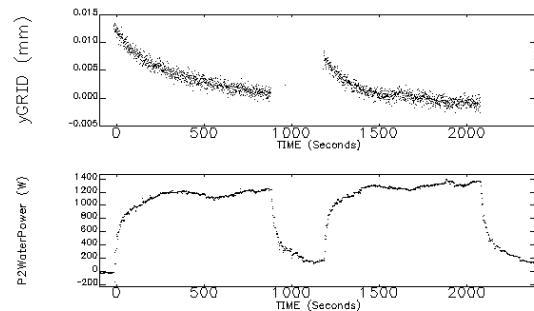


Figure 8: Upper panel: Thermal transient in XBPM after opening the photon shutter. Lower panel: Power carried by cooling water.

### SUMMARY

We performed the first high-power tests on the GRID-XBPM and demonstrated the following: (1) GRID-XBPM has lower signal background by one to two orders of magnitude compared with photoemission XBPMs. (2) Center-of-mass measurements can be performed in one dimension with gap dependence as little as  $\pm 2\%$  using normal machine shop and alignment tools. (3) Monochromatic beam profiles clearly correlate strongly with the XRF XBPM measurements, which can be used in the machine orbit feedback. (4) Thermal measurements showed the need to add additional water-cooling to maintain temperature stability of the chamber wall, detector, and supports.

### REFERENCES

- [1] B. X. Yang, G. Decker, S. H. Lee, and P. Den Hartog, "High-power hard x-ray beam position monitor development at APS," BIW'10, Santa Fe, May 2010, p. 233 (2010); <http://www.JACoW.org>.
- [2] B.X. Yang, G. Decker, S. H. Lee, P. Den Hartog, and K. W. Schlax, "Progress in the development of a grazing-incidence insertion device x-ray beam position monitor," PAC'11, New York, p. 443 (2011).
- [3] G. Decker, O. Singh, "Method for Reducing X-ray Background Signals from Insertion Device X-ray Beam Position Monitors," Phys. Rev. Spec. Top., Accel. Beams 2 (11), 112801 (1999).